
Article:
Lin, L., Miao, N., Huang, J. et al. (6 more authors) (2017) A photocatalyst of sulphur depleted monolayered molybdenum sulfide nanocrystals for dye degradation and hydrogen evolution reaction. Nano Energy, 38. pp. 544-552. ISSN 2211-2855

https://doi.org/10.1016/j.nanoen.2017.06.008

A photocatalyst of sulphur depleted monolayered molybdenum sulfide nanocrystals for dye degradation and hydrogen evolution reaction

Liangxu Li[a,b], Naihua Miao[c,d], Juntong Huang[a,e], Shaowei Zhang[a,*], Yanqiu Zhu[a], David D. Horsell[a], Philippe Ghosez[d], Zhimei Sun[c], and Dan A. Allwood[b,*]

[a]College of Engineering, Mathematics and Physical Sciences, University of Exeter, Exeter, EX4 4QL, UK
[b]Department of Materials Science and Engineering, University of Sheffield, Sheffield, S1 3JD, UK
[c]School of Materials Science and Engineering, Beihang University, Beijing, 100191, China
[d]Theoretical Materials Physics, Institut de Physique, Université de Liège, Liège, B-4000, Belgium
[e]School of Materials Science and Engineering, Nanchang Hangkong University, Nanchang, 330063, China

Abstract: Molybdenum disulfide (MoS_2) has a theoretical catalytic activity comparable to Pt but in practice is a poor catalyst in bulk form due to the scarcity of metal edge sites and low electrical conductivity. Recent developments on MoS_2 monolayers (MLs) are more encouraging in developing cheap and efficient catalysts, but the majority metal atoms are on the basal plane are catalytically inactive. The rapid recombination of the electron-hole pairs and electronic band structure of the most stable 2H-MoS_2 MLs are also unsuitable for efficient photocatalysis, especially for solar-driven water splitting. Here, we show that reducing the lateral size and creating sulphur (S) vacancies of MoS_2 MLs not only increases dramatically the density of catalytically active sites, but also adjusts the band structure to become highly suitable for solar-driven catalysis. Besides, this preparation efficiently avoids fast charge recombination associated with MoS_2, improves light harvesting, and gives a newly formed metallic state to transfer electrons for photocatalytic reactions. By way of example, we have demonstrated remarkable photocatalytic degradation of methylene blue (MB) and methylene orange (MO) dye using the S-depleted Mo-S nanocrystals (NCs, 2-25 nm). The NCs are also promising to efficiently generate hydrogen (H_2) from water with sacrificial reagents and solar light irradiation. Our study shows how careful design and modification of materials can result in highly efficient photocatalysts, which give considerable opportunities of the transition metal dichalcogenides (TMDs) beyond just MoS_2 to develop highly efficient and economic catalysts.

Keywords: Monolayered molybdenum disulfide, Nanocrystals, Photocatalyst, Electronic structure, Hydrogen evolution reaction

1. Introduction

Catalysts promise to play a vital role in addressing the pressing energy and environmental crises affecting our society, but the most effective catalysts are based on expensive and rare precious metals such as Pt and Au. Calculations suggest that transition metal dichalcogenides (TMDs) may offer cheaper and more readily available catalyst [1]. For example, MoS_2 nanoparticles or nanoflakes have significant catalytic activity and have been used in hydrogen evolution [2,3] and low carbon alcohol synthesis reactions [4]. However, the catalytic activity of MoS_2 is poor in practice due to the low charge mobility and scarcity of metal edge sites which are the only catalytically active part of the material [5-10]. Improvements in MoS_2 catalytic performance have been made by increasing the number of exposed edge sites [3-8], and with monolayered MoS_2 sheets with increased electrical conductivity but the majority of metal on the basal plane of MLs still remains catalytically inactive [11-13]. The direct semiconductor nature[13] of the most stable 2H-MoS_2 MLs and defect levels lying lower than the potential for water reduction [15,16] also restrict their photocatalytic efficiency, especially for the hydrogen evolution reaction (HER) from water.

Previously, we have achieved high yield monolayered 2H-MoS_2 NCs (2-25 nm width, average size ~12.9 nm) with a simple method, which involves the intercalation of bulk layered MoS_2 with potassium. De-intercalation of the K intercalated MoS_2 in H_2O/EtOH solvent under ultrasonication led to the exfoliation and disintegration of MoS_2 to monolayered NCs (Fig. 1a, also see Method) [17]. S-depletion of NCs using a cation exchange resin (Fig. 1a; further see Method and Supplementary Fig. S1) has led to stable 2H-$MoS_{1.65}$ NCs with superelectrochemical performance for HER [17]. The improvement of the electrochemical performance was mainly due to the increased number of catalytically active sites. Here, with same S-depleted NCs ($MoS_{1.65}$), we show that S-vacancies and a metallic nature (semiconducting core with metallic edge and shell) also make monolayered Mo-S NCs highly efficient photocatalysts for both dye degradation and hydrogen generation. Besides the increased density of catalytically active sites (compare with large MLs), new trapping and metallic sites created by S vacancies promote photogenerated carrier separation and prevent them from rapid recombination during photocatalytic reactions. The enlarged band gap (compare with large MLs) of monolayered NCs, due to quantum confinement effects, also makes them highly promising photocatalysts for HER.

2. Experimental

2.1 Preparation of monolayered Mo-S NCs

MoS_2 and S-depleted NCs are the same to that used in our previous work [17]. The monolayered MoS_2 NCs were created via exfoliation and disintegration of MoS_2 layers. As demonstrated in Fig. 1a, K was intercalated into the interlayer of MoS_2 flakes via heating reaction under vacuum conditions. The K intercalated MoS_2 was reacted with EtOH/H_2O with ultrasonication, which exfoliated and disintegrated monolayered MoS_2 NCs. The formed monolayered MoS_2 NCs were then separated with residual MoS_2 flakes via

centrifugation (Supplementary Fig. S1a-b). EtOH in NCs suspension was evaporated, and K^+ was removed by either dialysis or cation exchange resin. Upon the reaction with the cation exchange resin, removal of K^+ was accompanied by NCs changing to a dark color and undergoing partial S-depletion (H_2S formed during this treatment; Supplementary Fig. S1c). Fig. S1d shows the reaction of MoS_2 NCs with the cation exchange resin (left image: MoS_2 NCs; right image: 30 seconds after the mixture of MoS_2 NCs with resin). The S-depleted NCs are thermal unstable and could agglomerate together under high concentration and heating (Supplementary Fig. S1e, left side). However, these could be diluted and re-dispersed again with simple ultrasonication treatment (Supplementary Fig. S1e, right side). The agglomerated S-depleted Mo-S NCs can be collected as powder (Supplementary Fig. S1f) for characterization. Our previous characterization showed that the exfoliated and disintegrated NCs are monolayered MoS_2 with highly crystallized 2H structure, clearly terminated edges and strong luminescence (quantum yield = 7.9 %) [17]. The S-depleted NCs were confirmed as $MoS_{1.65}$ with S vacancies on the basal plane and rough crystal edges [17].

2.2. Characterization

UV/Vis spectra were recorded from solutions using a PerkinElmer Lambda 900 Spectrometer (10 mm cuvette light path) at room temperature. Raman spectra were recorded on a Renishaw in plus laser Raman spectrometer with an excitation wavelength λ_{exc} = 514.5 nm. XPS was performed on a Kratos AXIS Nova X-ray photoelectron spectrometer with an excitation source of Al Ka. The binding energy of XPS was calibrated based on C1s (284.6 eV). Atomic force microscopy (AFM) was performed using a VEECO Dimension 3100 system in tapping mode. Transmission electron microscopy (TEM) images were obtained using a JEOL 2010F transmission electron microscope with a field emission gun operated at 200 kV. Photoluminescence (PL) spectra were recorded using a Hitachi F-4500 Fluorescence Spectrophotometer at 20 ^oC. Time resolved PL (TPRL) and PL excitation (PLE) spectra were recorded using an Edinburgh FS5 fluorescence spectrometer.

2.3. Photocatalytic degration of methylene bue (MB) and methyl orange (MO)

Solar-driven photocatalysis measurements were conducted by irradiating the sample with a Newport Oriel full spectrum solar simulator (92250A-1000, 1.5 G, 150 W Xenon lamp). The average intensity of irradiation on the solution surface was measured (at nine different positions) to be 5.2 $mW.cm^{-2}$ by an ILT 550-RAA spectroradiometer (International Light Technologies, measurement range from 250-900 nm). Before purification, the amount of KOH in the MoS_2 NC suspension was calculated from 0.6 g K which was used for the preparation of NCs [17]. Therefore, in the control experiment of $MoS_{1.65}$ NCs, the necessary addition of KOH into the NCs suspension was defined to keep same concentration to that of MoS_2 NCs before purification. Since we could not monitor the photodegration of MB (Sigma-Aldrich, product no: M9140) catalyzed by $MoS_{1.65}$ NCs with KOH by optical absorption effectively, we recorded a Supplementary Video to demonstrate how the MB was degraded rapidly. In this video, each addition of MB was of a concentrated solution containing an equal amount of MB to that used in the cycling experiment, which 100 mL of a dilute 20 ppm concentration of MB. We performed the video experiment by adding the concentrated MB into a $MoS_{1.65}$ NC suspension identical to that used in the cycling tests. We also estimated photocatalytic (driven either by full solar spectrum or visible light only with wavelengths < 390 nm cut off with 1 M $NaNO_2$, Sigma-Aldrich, product no: S2252) degration of MO (100 mL, 20 ppm, Alfa Aesar, product no: 17874) by monitoring the change in absorption of 465 nm wavelength light, with different amount of $MoS_{1.65}$ NCs (20 mg for solar-driven catalytic reaction, 5 mg for both solar and visible light-driven catalytic reactions). The content of the total organic carbon (TOC) in the reacted solutions were analyzed by HAD-2000A TOC analyzer.

2.4. Hydrogen generation measurement

The measurement was performed on a Shimadzu GC-2010 Plus gas chromatograph (GC) with a barrier ionization discharge (BID) detector. Hydrogen generation was performed in a 700 mL cylinder-shaped quartz container with an irradiation area of 19.6 cm^2. The quartz container had two side joint connections with one connected to a pure Ar (99.999%) source and the other to a GC instrument. The quartz container was initially evacuated and then replaced by the pure Ar. The solution was then gently stirred with a magnetic stirrer with air flow cooling (20 ^oC) and irradiated using an AM 1.5G solar simulator as the light source (Newport Oriel full spectrum solar simulator, 150 W Xenon lamp) with and without a 350 nm long-pass cut off filter. Before each sampling, a low flow of Ar (5 mL/min) was introduced into the container and the outlet gas was measured by gas chromatography (GC). After each test, the solar simulator was switched off and the gas inside the quartz was replaced and purged by high flow (200 mL/min) for 10 minutes before the reactor was irradiated again and the reaction time was counted sequentially. During breaks in the cycling test, the quartz container was kept in a completely dark environment. Further experiments followed this procedure but with the addition of a 420 nm long-pass filter to remove all UV light irradiation. As for D_2O experiment, it was the same as the standard hydrogen generation experiment above, except the H_2O was replaced by D_2O. Before the experiment, the catalyst suspensions was repeatedly distilled with a rotary evaporator and replaced by absolute ethanol. After running for 10 h, the gas inside the reactor was carried to (with 10 mL/min air) and measured by Hiden Analytical's QGA for detection of H_2 and D_2.

2.4. Electrochemical measurement

All the electrochemical measurements were performed on a CHI 650C electrochemical workstation with three electrodes [reference electrode: Ag/AgCl, 1M KCl, E (potential) = 0.235 V vs RHE (reversible hydrogen electrode); counter electrode: Pt; working electrode: ITO (indium tin oxide coated glass)]. Photo-generated current was measured with a 0.5 M KCl electrolyte. Identical massed of MoS_2 and S-depleted $MoS_{1.65}$ NCs (around 0.57 mg) was deposited on separate 1 × 1 cm^2 area ITO surfaces and then air-dried overnight. Electrochemical measurements were performed with a bias voltage of 0.1 V with and without AM 1.5G solar light illumination (Newport Oriel full spectrum solar simulator, 150 W Xenon lamp) in an otherwise dark environment. Mott-Schottky analysis was performed using impedance-potential technique and 0.5 M KCl

electrolyte (pH close to 7) and a scan frequency of 10 Hz. AC impendence measurements were carried out at 80 mV overpotential and a frequency range from 105 Hz to 0.01 Hz. Double layer capacitance (C_{dl}) of NCs before and after S-depletion was estimated by capacitance-voltage (CV) measurements at scan rates of 60, 100, 140 and 180 $mV.s^{-1}$ with potential range of 0.035-0.235 V (1 M H_2SO_4). The slop of the plot, the difference between anodic and cathodic currents at 0.15V (vs RHE, 0.15 V was normally used in the measurement for MoS_2 materials [17]) against different scan rates, is C_{dl}. 5 µL ~275 µg/mL (see Supplementary Methods for the confirmation of the mass and concentration) NCs were immobilized on electrode for the above impedance and CV measurements. In these measurements, the potential, $E_{(RHE)}$, was calculated with the Nernst equation:

$$E_{(RHE)} = E_{(Ag/AgCl)} + 0.059 \times (pH) + 0.235$$

where $E_{(RHE)}$ is the potential versus RHE, $E_{(Ag/AgCl)}$ is the potential of reference electrode versus RHE, pH is the pH value of the electrolyte.

3. Results and discussions

3.1. Characterizations of monolayered Mo-S NCs.

The treatment of NCs with cation exchange resin has led to the removal of ~18% S from MoS_2, giving chemical composition of $MoS_{1.65}$ (Supplementary Fig. S2a, the XPS survey). We characterized the prepared $MoS_{1.65}$ NCs before the demonstration of the photocatalytic performance. As shown in TEM (Fig. 1b) and AFM images (Fig. 1c), the NCs have a diameter around 2-25 nm. Fig. 2 highlights three typical Mo-S NCs with thickness around 1 nm, corresponding to that of monolayers [18] (EDS of these NCs is shown in Supplementary Fig. S2b). These prepared $MoS_{1.65}$ NCs are still crystallized, though point defects are commonly found in HRTEM image (Fig. 1d). More structural information in Fig. 1e further revealed defects and rough edge of the NC. Nevertheless, confirmed by fast Fourier transform (FFT) patterns (Fig. 1e inset), the NC still exhibits hexagonal structure of 2H-MoS_2.

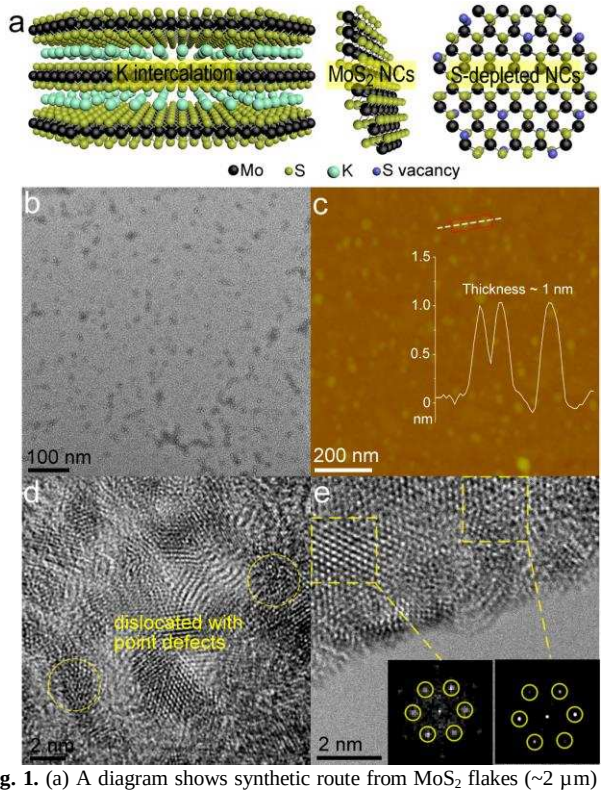

Fig. 1. (a) A diagram shows synthetic route from MoS_2 flakes (~2 µm) to monolayered MoS_2 NCs (the intercalated K reacted with $EtOH/H_2O$, exfoliated and disintegrated MoS_2 sheets to monolayered NCs under ultrasonication), and to monolayered $MoS_{1.65}$ NCs with S vacancies (partial S atoms were removed by cation exchange resin); (b-e) TEM image (c), AFM image (c), HRTEM images (d,e) and FFT patterns (d inset) of the $MoS_{1.65}$ NCs.

The 2H structure of NCs was further confirmed by Raman and XPS analyses. As shown in Fig. 2a, Raman spectroscopy showed that the underlying 2H crystal structure of the original raw materials remained in NCs, with E^1_{2g} at 382.2 cm^{-1} and A_{1g} Raman modes at 402.6 cm^{-1}, corresponding to those of 2H-MoS_2 [18]. Fig. 2b and c are the S(2p) and Mo(3d) XPS of the $MoS_{1.65}$ NCs, respectively. Deconvolution of the spectra gave S $2p_{3/2}$ (162.2 eV), S $2p_{1/2}$ (163.4 eV), Mo $3d_{3/2}$ (232.3 eV) and Mo $3d_{5/2}$ (229.2 eV), which well correspond to the XPS of 2H-MoS_2 [18,19]. In the prepared $MoS_{1.65}$ NCs, The oxidation state of Mo and S should be minimal due to the absence of prominent peaks at around 236 eV of Mo(3d) and 168-170 eV of S(2p) [18,19]. Besides, the NCs exhibited defect states, whose S 2p, Mo $3d_{3/2}$ and Mo $3d_{5/2}$ are found at 163.9, 233 and 229.8 eV respectively (Fig. 2b and c) and close to that previously discovered in defect-containing Mo-S NCs [19]. In the Mo (3d) XPS spectrum, there are another two peaks at 231.9 and 228.7 eV, which should be raised from the metallic phase on $MoS_{1.65}$ NCs [19]. These metallic phases were also discovered in pure NCs without S-depletion [17] and will be important for photocatalytic reactions.

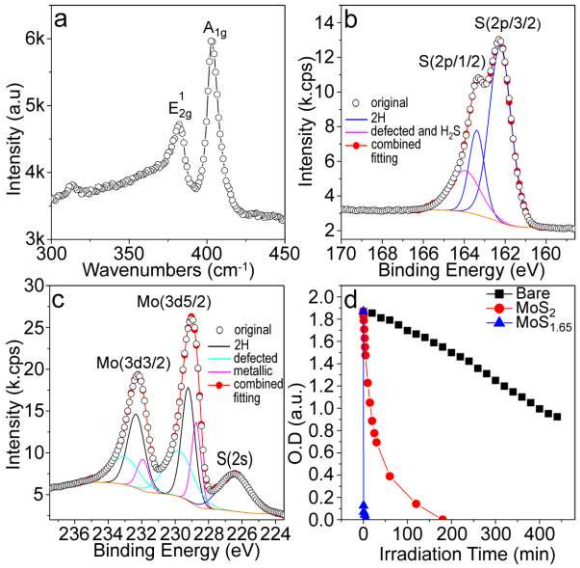

Fig. 2. (a-c) Raman (a) and XPS spectra (b-c) of the prepared $MoS_{1.65}$ NCs; (d) Comparison of the solar-driven self-degradation of MB, and photo-degradation of MB catalyzed by MoS_2 and S-depleted $MoS_{1.65}$ NCs under same experimental conditions, shown as OD_{670} of the MB solution as a function of irradiation time.

We compared the UV/Vis (ultraviolet to visible) spectra of monolayered Mo-S NCs before (MoS_2) and after S-depletion ($MoS_{1.65}$). Our spectroscopy of 2H-MoS_2 NCs suggested three evident absorption peaks at around 470 (2.64 eV), 390 (3.12 eV) and 318 nm (3.90 eV) (Supplementary Fig. S3c), which might be the excitonic absorption peaks (A, B and C at K point of the first Brillouin zone from low to high energy) [14] and close to that discovered in 2H-MoS_2 nanoclusters (~4.0-4.5 nm in diameter) [20]. Unlike pure MoS_2 NCs (without S-depletion) with relative weak absorption of visible light (Supplementary Fig. S3a-b), the $MoS_{1.65}$ NCs can strongly absorb visible light, which is also reflected by the dark brown color of $MoS_{1.65}$ NCs (initial MoS_2 NCs are faint yellow; Supplementary Fig. S1). The increased absorption of S-depleted NCs from initial MoS_2 NCs at visible light region is believed as the result of the formation of new in-band defect levels (will be further confirmed in detail). These new defect levels make excitonic absorption peaks of S-depleted NCs unconspicuous, leaving a wide absorption tail from 2-5 eV and an absorption edge close to 2 eV (Supplementary Fig. S3d). The defect level also quenched photon recombination of NCs (no clear luminescence of $MoS_{1.65}$ NCs was found with excitation wavelength from 200-900 nm), and should benefit to photocatalytic reactions. By contrast, pure monolayered MoS_2 NCs have intense luminescence (quantum yield of ~7.9%), as we previously discovered [17]. It is well know that MoS_2 monolayers are direct semiconductor with photoluminescence (PL) generated by the recombination from A and B excitations (A and B excitations are the spin-split of the conduction band in monolayers) [14]. We further conducted a series of PL and PL excitation (PLE) measurements of MoS_2 NCs, which confirmed that the luminescence is mainly contributed by the recombination from the energy levels at around 470 (2.64 eV) and 390 nm (3.12 eV), respectively (see Supplementary Fig. S4 for details). This confirms that the discovered absorptions at around 470 (2.64 eV) and 390 nm (3.12 eV) are excitations A and B respectively, and suggests an average optical band of around 2.9 eV (average value of the excitations A and B) of monolayered MoS_2 NCs. The high photon recombination rate (quantum yield of ~7.9%) from excitations A and B, and large band gap (~2.9 eV) of monolayered MoS_2 NCs means that the photocatalytic activity of Mo edges would be largely suppressed. Nevertheless, S-depleted Mo-S NCs may be promising materials to capture and convert solar energy for practical uses (e.g. photocatalyst and solar-cell) because of the possible formed defect levels.

3.2. Highly efficient photocatalytic dye degradation using of monolayered Mo-S NCs

We investigated solar-driven photocatalysis using S-depleted monolayered $MoS_{1.65}$ NCs by monitoring the photocatalytic degradation of a methylene blue (MB) solution using the change in absorption of the main characteristic peak (670 nm). 20 mg $MoS_{1.65}$ in 75 ml water (see Supplementary Methods for mass calculation) was dispersed in a beaker (inner diameter of 5 cm) under simulated solar irradiation (1.5G) with magnetic stirring at room temperature (20 ^oC). Then, 25 ml 80 ppm fresh MB was added to the beaker to form an overall concentration of 20 ppm with an initial optical density (OD_{670}) of 1.87 (~5.2 $mW.cm^{-2}$ of incident irradiation intensity). Control measurements of MB under identical conditions were performed but with the $MoS_{1.65}$ NCs either removed completely or replaced by 20 mg MoS_2 NCs (before S-depletion, including KOH in the solution since it is difficult to remove without loss of the NCs). With no NCs, the photodegradation of MB was slow [e.g. only 50% was degraded after 440 mins (Fig. 2d)]. Inclusion of the stoichiometric MoS_2 NCs resulted in complete MB photodegradation after 180 mins but when catalyzed by S-depleted $MoS_{1.65}$ NCs this was complete in only 7 mins (Fig. 2d). TOC of the reacted solution (with $MoS_{1.65}$ NCs catalyst) was measured as around 0.34 mg/L, which means that over 97% MB (in 100 mL solution) was completed degraded during the catalytic reaction. To check the influence of KOH on the reaction with the low defect MoS_2 NCs, photocatalytic measurements using S-depleted $MoS_{1.65}$ NC with added KOH (same concentration as the NC suspension, see Method) resulted in the MB degrading within only a few seconds (Supplementary Video) and too rapidly for us to monitor effectively (this catalytic performance is far beyond the most developed catalysts). This improvement is understandable since OH^- suppressed the agglomeration of $MoS_{1.65}$ NCs, and improved the adsorption of MB (positively charged) by $MoS_{1.65}$ NCs (positively charged). We performed cycling tests of the solar-driven degradation of MB catalyzed by $MoS_{1.65}$ NCs (no addition of KOH). Following the full degradation of MB from a previous cycle, the $MoS_{1.65}$ NCs were re-dispersed by ultrasonication and the next cycle started after 1 mL 2000 ppm fresh MB was added to restore its concentration to 20 ppm. The high repeatability of the photodegradation over eight cycles (Supplementary Fig. S5a) demonstrates that the photocatalytic activity of S-depleted $MoS_{1.65}$ NCs remains stable under solar irradiation.

The S-depleted NCs also showed remarkable photocatalytic behavior in the degradation of more stable methyl orange (MO). With 20 mg $MoS_{1.65}$ NCs, we found that MO (100 mL, 20 ppm) fully degraded within 3 mins (Fig. 3a), which is more rapid

than the degradation of MB (20 ppm in 7 mins; MO are negative charged leading to adsorption by positive charged $MoS_{1.65}$ NCs). Only ~0.2 mg/L TOC was remained in the reacted solution, which suggest that over 98% MO was completed degraded. The photodegradation of MO catalyzed by $MoS_{1.65}$ NCs is far more rapid than other photocatalysts [21,22]. For example, degradation of 100 mL 20 ppm MO required hours under 300 W UV irradiation with 20 mg nitrogen-fluorine co-doped TiO_2 catalyst [22]. Even with a low concentration of $MoS_{1.65}$ NCs (5 mg), fully degradation of MO only required 24 and 28 mins under full-solar and visible-solar (wavelength > 390 nm only; λ < 390 nm was cut off by 1M aqueous $NaNO_2$ solvent; the cut off efficiency has been already confirmed in our previous report [21]) light irradiation, respectively (Supplementary Fig. S5b-c).

3.3. Efficient solar-driven hydrogen evolution reaction of monolayered Mo-S NCs.

The monolayered $MoS_{1.65}$ NCs are also efficient photocatalysts of H_2 generation from water. We placed 20 mg $MoS_{1.65}$ NCs in a quartz cylinder with 450 mL of different aqueous solvents to leave 250 mL head space in the container before irradiating the top surface (5 cm efficient irradiation diameter, ~4.7 $mW.cm^{-2}$ on the top of solution inside the cylinder) with a solar simulator (1.5G) at room temperature (20 ^oC). A 5 mL/min flow of pure Ar (99.999%) was passed through the quartz container and its content from the reaction vessel measured by gas chromatography (GC, see Method for details). A methanol solvent (100 mL methanol, 350 mL deionized water, pH adjusted to 13 by KOH to improve the dispersity of NCs) achieved H_2 production of 8.4 $\mu mol.hour^{-1}$. By comparison, using non-S-depleted MoS_2 NCs under otherwise identical experimental conditions produced negligible H_2, possibly due to the large optical band gap (2.9 eV) and high photon recombination rate (quantum yield = 7.9%) of these NCs. Negligible H_2 was produced when using S-depleted NCs in pure water (350 mL, Mo and S were also slightly oxidized after days reaction, Supplementary Fig. S6a-b), but H_2 production could be restored once 100 mL methanol was added, suggesting the methanol acts sacrificially to remove liberated oxygen, suppress O_2 formation and restore the catalytic activity of the active sites. We further verified that the detected H_2 was indeed generated by water splitting by replacing H_2O with D_2O and observing only D_2 was detected by mass spectrometry (Supplementary Fig. S6c).

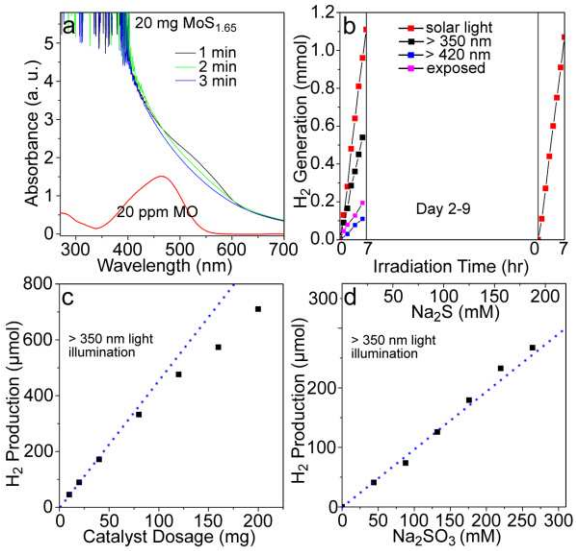

Fig. 3. (a) Solar-driven photo-degradation of MO (100 mL, 20 ppm) catalyzed by 20 mg $MoS_{1.65}$ NCs; (b) Cycling (the 1st and 11st day) measurements of solar-driven hydrogen gas generation from water with $MoS_{1.65}$ NCs. Also shown in the 1st day is solar-driven H_2 generation with irradiation wavelengths above 350 nm (black dot) and 420 nm (blue dot), and H_2 generation with irradiation wavelengths above 350 nm without Ar purge (purple dot); (c) Relationship between H_2 production in 1 h and catalyst dosage; (d) Relationship between H_2 production in 2 h and the concentration of Na_2SO_3/Na_2S complex.

The rate of H_2 production with S-depleted $MoS_{1.65}$ NC catalysts could be increased with the use of other sacrificial reagents. Aqueous lactic acid (13 mL lactic acid, 437 mL deionized water, adjusted to pH 4 by KOH) resulted in H_2 evolution of 34.6 $\mu mol.hr^{-1}$ while this reached 160 $\mu mol.hr^{-1}$ using aqueous Na_2SO_3/Na_2S [450 mL deionized water, 10 g Na_2SO_3 (0.176 M) and 4.4 g Na_2S (0.125 M); again, the sacrificial reagents prevented O_2 generation (Supplementary Fig. S6d)]. The large improvement of the H_2 production in Na_2SO_3/Na_2S should be also contributed by the high pH (>7) value which benefited the dispersity of positive charged NCs. We conducted H_2 gas evolution for eleven days (~7 hours each day; sample stored in darkness between reactions each day) and found that the $MoS_{1.65}$ NCs exhibited a nearly unchanged rate of H_2 production through this time (see Fig. 3b to compare the 1st and 11st day). During this experiment, the solvent pH increased to ~14, which should assist the catalytic activity of the NCs. It is not clear whether this pH change was due to the consumption of sacrificial reagents. After catalytic reaction, SO_4^{2-} and $S_2O_3^{2-}$ were produced in N_2SO_3/Na_2S solution (analysis followed the reported method [23]), which is the same to the previous report on the photocatalytic hydrogenation evolution reaction with N_2SO_3/Na_2S solution [23-25]. XPS, UV/Vis, and Raman analyses of the NCs (>85% NC collected) after this time plus 6 months in darkness also show they have good stability with 2H semiconductor structure remained (Supplementary Fig. S6a-b and Fig. S7a-b).

Table 1. Catalytic performance for H_2 production of different catalysts (AM 1.5 G).

Catalyst	Lamp: mW/cm^2	H_2 Production ($\mu mol.hr^{-1}.g^{-1}$)		
		>300 nm	>350 nm	>420 nm
Mo-S NCs	4.7 (150 W)		4460	940

ZnO [27]	1.0 (300 W)	293
B-ZnO [27]	1.0 (300W)	576.6
C-CdO [25]	-- (300 W)	3
ZnS/graphene/ MoS_2 [28]	125 (300W)	2258 (full light irradiation)
MoS_2/TiO_2 [29]	600 (300W)	1600 (full light irradiation)

However, the above H_2 production will be an overestimate since the photochemical reaction of Na_2SO_3/Na_2S also generates H_2 [we also found H_2 generated with H_2S production (Supplementary Fig. S7c)] [24]. Removing light below 350 nm wavelength (similar to others for HER in Na_2SO_3/Na_2S) [24] with an optical filter avoided photoreactions of sacrificial reagents (H_2 generation from aqueous Na_2SO_3/Na_2S alone became negligible) but reduced the H_2 production rate to 89.2 $\mu mol.hr^{-1}$ (Fig. 3b and Supplementary Fig. S7d), i.e. 4460 $\mu mol.hr^{-1}.g^{-1}$ of $MoS_{1.65}$ NC photocatalyst (represents an efficient photocatalytic H_2 generation from water). It also linearly reduced with the decrement of light intensity (> 350 nm; quartz cover was applied to reduce the light intensity; see Supplementary Fig. S8 for details). The H_2 production rate further reduced to 32.3 $\mu mol.hr^{-1}$ under aerobic conditions (no Ar purge was used, Fig. 3b). With identical light irradiation (>350 nm), we found that the H_2 production rate is highly dependent on the concentration of both the NCs and the Na_2SO_3/Na_2S sacrificial reagents. As shown in Fig. 3c, the H_2 production in 1 h linearly increased with the dosage of NCs < 40 mg, but the H_2 production rate per gram catalyst gradually reduced with more NCs added (> 40 mg/mL). This phenomenon is reasonable since more added NCs gave a darker solution, which reduced light transmittance of the solution. Fig. 3d shows the relationship between the H_2 production in 2 h and the concentration of Na_2SO_3/Na_2S (20 mg NCs). In the studied range, the H_2 production nearly linearly increased with the concentration of Na_2SO_3/Na_2S complex (the linear dependency is similar to previous reports [26]). The irradiation light with wavelengths below 420 nm was further filtered to study the visible-light driven catalysis. In this case, a H_2 production of 18.8 $\mu mol.hour^{-1}$ was still achieved (Fig. 3b), reflecting the activity of the intermediate band gap states of $MoS_{1.65}$ NCs. The above catalytic performance for H_2 production is much higher than that of many other reported catalysts with similar Na_2S/Na_2SO_3 sacrificial reagents (see Table 1). For example, the hybrid material of ZnS, graphene and MoS_2 has H_2 production of 2258 $\mu mol.hr^{-1}.g^{-1}$ with incident light intensity of 125 mW/cm^2 [28], whilst our prepared Mo-S NCs yield 4460 and 940 $\mu mol.hr^{-1}.g^{-1}$ H_2 at wavelength > 350 and > 420 respectively (incident light intensity ~4.7 $mW.cm^{-2}$).

3.4. Defect levels of monolayered Mo-S NCs for highly efficient photocatalysis

Our previous study suggests that MoS_2 NCs appears to be metallic, and the metallicity is improved by S-depletion [17]. The metallic character is limited to the NC edge and near-edge regions while the inner NC core remains semiconducting, recovering electronic properties close to those of MoS_2 monolayers (MLs) [17]. We found here through photocurrent measurements (Supplementary Fig. S7e) that the improved metallicity of $MoS_{1.65}$ NCs compared to pure MoS_2 NCs efficiently increased the NCs' photo-activity. However, the improved metallicity is insufficient to explain the remarkable photocatalysis of S-depleted Mo-S NCs. The improved light absorption at visible light region of Mo-S NCs upon S-depletion (the introduction of defect levels) should be fully considered.

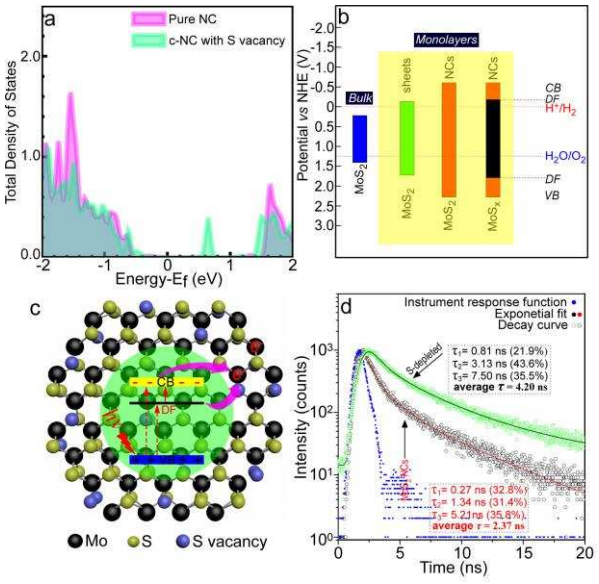

Fig. 4. (a) Calculated DOS of pure MoS_2 and the core of the S-$MoS_{1.65}$ NCs. The DOS unit is states.eV^{-1}f.u.$^{-1}$ (f.u.: formula unit); (b) Diagram of the band position change of MoS_2 from bulk to monolayers. The conduction band (CB), valence band (VB) and defect levels (DF) are shown in the diagram. The calculated CB and VB of pure NCs from are around -0.6 and 2.3 eV, respectively. The band edge of bulk phase and monolayered sheets are presented based on the reported data [15,16]; (c) Schematic illustration of the photo-reaction on a s-depleted Mo-S NC; (d) Time-resolved photoluminescence (TRPL) spectra of MoS_2 (emission ~ 470 nm) and $MoS_{1.65}$ NCs (emission ~ 580 nm) with 360 nm wavelength optical excitation.

To understand the intra-band transitions of $MoS_{1.65}$ NCs and the photocatalysis improvement upon the S-depletion, we calculated the electronic band structure of NCs before and after S-depletion from density functional theory using a projector-augmented wave method [30] as implemented in the Vienna ab initio Simulation Package (VASP) [31] (details in Supplementary Method). We predict here a fundamental band gap (different with optical band gap) of ~2.0 eV of NCs, which is slightly larger than that of MLs (1.7 eV, Supplementary Fig. S9) within the local density approximation (LDA). The latter is known, however, to systematically underestimate band gaps [32]. As suggested by previous GW calculations and further supported here by our hybrid functional calculations (HSE, see Supplementary Fig. S9), the correct value should be 0.7-1.0 eV larger [32,33]. This corresponds to a fundamental band gap in the range 2.7-3.0 eV, which is fully compatible with the optical measurements we described previously (~2.9 eV), assuming that excitonic binding energies are strongly reduced in NCs compared to MLs. Such a reduction in NCs is expected from the presence of a metallic surrounding region [34].

The existence of mono-S vacancies in the core region of NCs (c-NCs) slightly reduces the band gap (0.2 eV) and induces the appearance of in-gap electronic defect states, located ~0.7 eV below the bottom of the conduction band bottom of MoS_2 c-NCs (Fig. 4a). This location is robustly predicted in our calculations and is independent of the functional used (LDA or HSE, Supplementary Fig. S9). It is also comparable to the

location of mono-S vacancies in MoS_2 MLs (~0.6 eV below the bottom of the conduction band) [16]. Adding S vacancies in the edge regions of NCs does not affect further the electronic properties of the core region (Fig. 4a). The intra-band transitions of $MoS_{1.65}$ NCs are, therefore, likely to involve these vacancy-induced raised defect levels to give increased optical absorption in the visible region (Supplementary Fig. S3a-b). The ~2.9 eV band gap of MoS_2 NCs as suggested from our optical absorption measurements above might be too large for efficient solar-driven catalysis. Assuming that the core S-vacancies slightly reduce the band gap (0.2 eV) and create defect states 0.7 eV below the calculated conduction band minimums (CB), these defect states will lie ~2.0 eV above the valence band maximum (VB). This corresponds to a reduced effective band gap in the S-depleted $MoS_{1.65}$ NCs very close to the optimal gap value for solar-driven catalytic applications. Our PLE (Fig. 5a) investigation of the $MoS_{1.65}$ NCs suggest three excitation peaks at around 413 (3.0 eV), 502 (2.47 eV) and 601 nm (2.06 eV) with detection wavelength of 660 nm (close to maximum emission position, though the PL is negligible). In this spectrum, the observation of the PLE peak at around 538 nm is due to the Raman response of H_2O at around 660 nm (verified with pure H_2O). The peaks at around 413, 502, and 601 nm can be attributed to the shifted B and A excitations and new defect levels, respectively. Therefore, the average optical band gap (A and B peak at K point) of the $MoS_{1.65}$ NCs changed to around 2.74 eV (from ~ 2.9 of MoS_2 NCs) with a defect level 0.68 eV below, which is very close to above calculations (0.7 eV below the CB) and highly suitable for solar-driven catalytic reactions.

3.5. Band edge positions of monolayered Mo-S NCs for highly efficient HER

We have further evaluated the positions of the band edges of $MoS_{1.65}$ NCs using an approach based on the band gap of semiconductors and the geometrical average of experimental electro-negativities of relevant atoms [35], which has been successfully applied to many semiconducting minerals including MoS_2 and TiO_2 [36]. The calculated effective conduction band and valence band edges potential of the NCs with S-vacancies are around -0.2 and +1.8 V, respectively (Fig. 4b, Supplementary Fig. S9). These cover the H_2O reduction/oxidation potentials (Fig. 4b), suggesting that the band edge positions of the $MoS_{1.65}$ NCs with respect to the normal hydrogen electrode (NHE) are ideally placed for photocatalytic hydrogen generation from water. Our Mott-Schottky plot of the $MoS_{1.65}$ NCs (Fig. 5b) shows the slope of n-type semiconductor. The flatband potential from this plot is around -0.1 V (vs NHE), which is the same as the Fermi level and close to the conduction band value (-0.2 V) in n-type semiconductors [37].

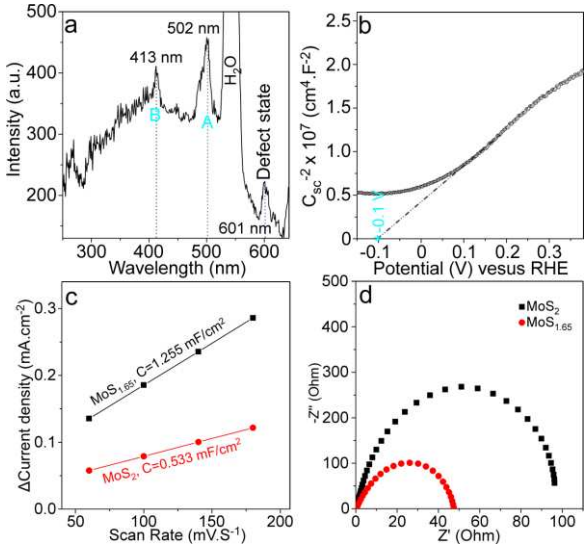

Fig. 5. (a) PLE spectrum of $MoS_{1.65}$ NCs with detection emission at around 660 nm (close to the maximum emission wavelength); (b) Mott-Schottky plot of the $MoS_{1.65}$ NCs suggests that the $MoS_{1.65}$ NCs are n-type semiconductor with minus slope and a flatband potential at around -0.1 V (this value is close to the conduction band position of n-type semiconductor); (c) Plots of capacitance from CV curves in Supplementary Fig. S10 giving capacitances of 0.533 and 1.255 mF/cm^2 for MoS_2 and MoS_1.65 NCs, respectively; (d) Nyquist plots showing EIS response with real (Z') and imaginary (Z'') impedance components of MoS_2 and $MoS_{1.65}$ NCs.

In addition to the change in band structure, S-depletion also increased the density of catalytically active Mo atoms and the metallicity (Supplementary Fig. S9). The increased density of catalytically active sites is confirmed by the double layer capacitance (C_{dl}) measurements (see Methods and Supplementary Fig. S10) with identical mass of NCs. As suggested in Fig. 5c, C_{dl} of $MoS_{1.65}$ (1.255 $mF.cm^{-2}$) increased from that of MoS_2 NCs (0.533 $mF.cm^{-2}$), which should linearly proportional to the number of catalytically reactive sites [17]. The increased metallicity is also confirmed by impedance spectroscopy (EIS) of both NCs with identical mass (see Methods), as the charger transfer resistances (R_{ct}) ~47 Ω of $MoS_{1.65}$ NCs decreased from 98 Ω of MoS_2 NCs. These metallic Mo sites are likely to serve as co-catalysts in a reaction, transferring electrons in the photocatalytic process (Fig. 4c) [38]. Fast charge recombination within $MoS_{1.65}$ NCs is also prevented by the metallic Mo sites and S-vacancy-related defect levels, giving increased relaxation time and higher photocurrent than that of MoS_2 NCs (Fig. 4d, Supplementary Fig. S7e). This combination of band gap, band edge position and defect states is likely to be the reason why H_2 can be produced from water (as well as the very rapid photo-degradation of organic pollutants) with S-depleted $MoS_{1.65}$ NCs as a photocatalyst and without recourse to further co-catalysts.

4. Conclusion

In summary, we have shown a feasible method (by size reduction and S-depletion) to increase the density of active sites and tune the electronic structure of MoS_2 monolayers for photocatalytic reactions. The prepared Mo-$S_{1.65}$ NCs (2-25 nm)

exhibited incredible activities on photo-degradations of methylene blue and methylene orange. It is also efficient to generate H_2 from mixed aqueous solution of Na_2SO_3 (0.176 M) and Na_2S (0.125 M), giving hydrogen production rate of 4460 and 940 $\mu mol.hr^{-1}.g^{-1}$ under irradiations (incident solar light intensity: 4.7 mW/cm^2) with wavelengths > 350 and >420 nm, respectively. We demonstrated how the size reduction into NCs and S-depletion of MoS_2 monolayers adjusted the band structure to become highly suitable for solar-driven catalysis (e.g. hydrogen evolution reaction). The monolayered MoS_2 NCs consist of metallic shell and 2H semiconducting core. MoS_2 NCs has an optical band gap ~ 2.9 eV which highly close to the real band gap due to the existence of metallic shell (excitonic binding energy strongly reduced). S-depletion of NCs increased metallicity and reduced the effective band gap to ~ 2.0 eV, giving effective conduction and valence band edges potential at around -0.2 and +1.8 V, respectively. The defect states and metallic sites formed on monolayered S-depleted NCs also serve as co-catalysts in a reaction, transferring electrons in the photocatalytic process and preventing fast charge recombination. Our experimental and theoretical study here shows how careful modification of MoS_2 monolayers can result in highly efficient photocatalysis, and the avenues we have investigated may help in the development of cheap and effective non-precious metal based materials for catalysis. These results are also highly valuable in developing highly efficient energy harvesting system (e.g. hybrid Mo-S NCs and graphene structure building solar cell with high quantum efficiency).

Acknowledgement

We thank the National EPSRC XPS Users' Service (NEXUS) at the Newcastle University (UK) for the assistance with XPS characterizations.

Appendix A. Supplementary material

Supplementary data associated with this article can be found, in the online version, at xxxxxx.

References

[1] B. Hinnemann, P. G. Moses, J. Bonde, K. P. Jøergensen, J. H. Nielsen, S. Horch, I. Chorkendorff, J. K. Nørskov, Biomimetic hydrogen evolution: MoS_2 nanoparticles as catalyst for hydrogen evolution, J. Am. Chem. Soc. 127 (2005) 5308-5309.

[2] T. F. Jaramillo, K. P. Jøergensen, J. Bonde, J. H. Nielsen, S. Horch, I. Chorkendorff, Identification of active edge sites for electrochemical H_2 evolution from MoS_2 nanocatalysts, Science 317 (2007) 100-102.

[3] J. Xie, H. Zhang, S. Li, R. Wang, X. Sun, M. Zhou, J. Zhou, X. W. D. Lou, Y. Xie, Defect-rich MoS_2 ultrathin nanosheets with additional active edge sites for enhanced electrocatalytic hydrogen evolution, Adv. Mater. 25 (2013) 5807-5813.

[4] D. Le, T. B. Rawal, T. S. Rahman, Single-layer MoS_2 with sulfur vacancies: structure and catalytic application, J. Phys. Chem. C 118 (2014) 5346-5351.

[5] M. Chhowalla, H. S. Shin, G. Eda, L. -J. Li, K. P. Loh, H. Zhang, The chemistry of two-dimensional layered transition metal dichalcogenide nanosheets, Nat. Chem. 5 (2013) 263-275.

[6] H. I. Karunadasa, E. Montalvo, Y. Sun, M. Majda, J. R. Long, C. J. Chang, A Molecular MoS_2 edge site mimic for catalytic hydrogen generation, Science 335 (2012) 698-702

[7] J. Kibsgaard, Z. Chen, B. N. Reinecke, T. F. Jaramillo, Engineering the surface structure of MoS_2 to preferentially expose active edge sites for electrocatalysis, Nat. Mater. 11 (2012) 963-969.

[8] H. Wang, Z. Lu, S. Xu, D. Kong, J. J. Cha, G. Zheng, P.-C. Hsu, K. Yan, D. Bradshaw, F. B. Prinz, Y. Cui, Electrochemical tuning of vertically aligned MoS_2 nanofilms and its application in improving hydrogen evolution reaction, Proc. Natl. Acad. Sci. USA 110 (2013) 19701-19706.

[9] D. Voiry, J. Yang, M. Chhowalla, Recent strategies for improving the catalytic activity of 2D TMD nanosheets toward the hydrogen evolution Reaction, Adv. Mater. 28 (2016) 6197-6206.

[10] H. Li, C. Tsai, A. L. Koh, L. Cai, A. W. Contryman, A. H. Fragapane, J. Zhao, H. S. Han, H. C. Manoharan, F. Abild-Pedersen, J. K. Nørskov, X. Zheng, Activating and optimizing MoS_2 basal planes for hydrogen evolution through the formation of strained sulphur vacancies, Nat. Mat. 15 (2016) 48-53.

[11] D. Voiry, M. Salehi, R. Silva, T. Fujita, M. Chen, T. Asefa, V. B. Shenoy, G. Eda, M. Chhowalla, Conducting MoS_2 nanosheets as catalysts for hydrogen evolution reaction, Nano. Lett. 13 (2013) 6222-6227.

[12] Y. Yu, S.-Y. Huang, Y. Li, S. N. Steinmann, W. Yang, L. Cao, Layer-dependent electrocatalysis of MoS_2 for hydrogen evolution, Nano Lett. 14 (2014) 553-558.

[13] D. Voiry, R. Fullon, J. Yang, C. de Carvalho Castro e Silva, R. Kappera, I. Bozkurt, D. Kaplan, M. J. Lagos, P. E. Batson, G. Gupta, A. D. Mohite, L. Dong, D. Er, V. B. Shenoy, W. Asefa, M. Chhowalla, The role of electronic coupling between substrate and 2D MoS_2 nanosheets in electrocatalytic production of hydrogen, Nat. Commun. 15 (2016) 1003-1009.

[14] K. F. Mak, C. Lee, J. Hone, J. Shan, T. F. Heinz, Atomically thin MoS_2: a new direct-gap semiconductor, Phys. Rev. Lett. 105 (2010) 136805.

[15] H. Jiang, Electronic band structures of molybdenum and tungsten dichalcogenides by the GW approach, J. Phys. Chem. C 116 (2012) 7664-7671.

[16] W. Zhou, X. Zou, S. Najmaei, Z. Liu, Y. Shi, J. Kong, J. Lou, P. M. Ajayan, B. I. Yakobson, J.-C. Idrobo, Intrinsic structure defects in monolayer molybdenum disulfide, Nano Lett. 13 (2013) 2615-2622.

[17] L. Lin, N. Miao, Y. Wen, S. Zhang, P. Ghosez, Z. Sun, D. A. Allwood, Sulfur-depleted monolayered molybdenum disulfide nanocrystals for superelectrochemical hydrogen evolution reaction, ACS Nano 10 (2016) 8929-8937.

[18] G. Eda, H. Yamaguchi, D. Voiry, T. Fujita, M. Chen, M. Chhowalla, Photoluminescence from chemically exfoliated MoS_2, Nano Lett. 11 (2011) 5111-5116.

[19] M. A. Baker, R. Gilmore, C. Lenardi, W. Gissler, XPS investigation of preferential sputtering of S from MoS_2 and determination of MoS_x stoichiometry from Mo and S peak positions, Appl. Surf. Sci. 150 (1999) 255-262.

[20]J. P. Wilcoxon, P. P. Newcomer, G. A. Samara, Synthesis and optical properties of MoS_2 and isomorphous nanoclusters in the quantum confinement regime, J. Appl. Phys. 81 (1997) 7934-7944.
[21]L. Lin, J. Huang, X. Li, M. A. Abass, S. Zhang, Effective surface disorder engineering of metal oxide nanocrystals for improved photocatalysis, Appl. Catal. B-Environ. 203 (2017) 615-624.
[22] Z. He, W. Que, J. Chen, X. Yin, Y. He, J. Ren, Photocatalytic degradation of methyl orange over nitrogen-fluorine codoped TiO_2 nanobelts prepared by solvothermal synthesis, ACS Appl. Mater. Interfaces 4 (2012) 6816-6826.
[23]N. Bühler, K. Meier, J. Rober, Photochemical hydrogen production with cadmiun sulfide suspensions, J. Phys. Chem. 88 (1984) 3261-3268.
[24]H. Liu, W. Shanguan, Photochemical reduction and oxidation of water including sacrificial reagents and Pt/TiO_2 catalyst, Energ. Fuel. 20 (2006) 2289-2292.
[25]Q. Gu, H. Zhuang, J. Long, X. An, H. Lin, H. Lin, Enhanced hydrogen production over C-Doped CdO photocatalyst in Na_2S/Na_2SO_3 solution under visible light irradiation, Int. J. Photoenergy 22 (2012) 857345.
[26]H. Chen, Z. Sun, S. Ye, D. Lu, P. Du, J. Mater. Chem. A Molecular cobalt-salen complexes as novel cocatalysts for highly efficient photocatalytic hydrogen production over a CdS nanorod photosensitizer under visible light, J. Mater. Chem. A 3 (2015) 15729-15737.
[27]P. Gomathisankar, K. Hachisuka, H. Katsumata, T. Suzuki, K. Funasaka, S. Kaneco, Photocatalytic hydrogen production from aqueous $Na_2S + Na_2SO_3$ solution with B-doped ZnO, ACS Sustainable Chem. Eng. 1 (2013) 982-988.
[28]B. Zhu, B. Lin, Y. Zhou, P. Sun, Q. Yao, Y. Chen, B. Gao, Enhanced photocatalytic H_2 evolution on ZnS loaded with graphene and MoS_2 nanosheets as cocatalysts, J. Mater. Chem. A 2 (2014) 3819-3827.
[29]W. Zhou, Z. Yin, Y. Du, X. Huang, Z. Zeng, H. Liu, J. Wang, H. Zhang, Synthesis of few-layer MoS_2 nanosheet-coated TiO_2 nanobelt heterostructures for enhanced photocatalytic activities, Small 9 (2013) 140-147.
[30]P. E. Blöchl, Projector augmented-wave Method, Phys. Rev. B 50 (1994) 17953.
[31]J. Hafner, Ab-Initio simulations of materials using VASP: density-functional theory and beyond, J. Comput. Chem. 29 (2008) 2044.
[32]H. Shi, H. Pan, Y. Zhang, B. I. Yakobson, Quasiparticle band structures and optical properties of strained monolayer MoS_2 and WS_2, Phys. Rev. B 87 (2013) 155304.
[33]H. J. Conley, B. Wang, J. I. Ziegler, R. F. HaglundJr., S. T. Pantelides, K. L. Bolotin, Bandgap engineering of strained monolayer and bilayer MoS_2, Nano Lett. 13 (2013) 3626-3630.
[34]H. Komsa, A. Krasheninnikov, Effects of confinement and environment on the electronic structure and exciton binding energy of MoS_2 from first principles, Phys. Rev. B 86 (2012) 241201(R).
[35]R. G. Pearson, Absolute electronegativity and hardness: application to inorganic chemistry, Inorg. Chem. 27 (1988) 734-740.
[36]Y. Xu, M. A. A. Schoonen, The absolute energy positions of conduction and valence bands of selected semiconducting minerals, Am. Mineral. 85 (2000) 543-556.
[37]A. W. Bott, Electrochemistry of semiconductors, Current Separations 17 (1998) 87-91.
[38]J. Ran, J. Zhang, J. Yu, M. Jaroniec, S. Z. Qiao, Earth-abundant cocatalysts for semiconductor-based photocatalytic water splitting, Chem. Soc. Rev. 43 (2014) 7787-7812.